Complex Eruptive Dynamics Leading to a Prominence Eruption and a Partial-Halo Coronal Mass Ejection

M. Dechev[1], P. Duchlev[1], K. Koleva[1]
Institute of Astronomy and National Astronomical Observatory,
Bulgarian Academy of Sciences, 72 Tsarigradsko Shose blvd., 1784 Sofia, Bulgaria
mdechev@astro.bas.bg
(Submitted on 29.09.2017. Accepted on 7.12.2017)

Abstract. We present very rarely reported case of an eruptive prominence (EP) composed by both hot, bright flux rope (BFR) and cool massive flux ropes (MFR) and associated partial-halo coronal mass ejection (CME). Using SDO and STEREO A and B multi-wavelength observations, we examined in detail the eruption of EP flux ropes (FRs) and their associated activities in a complex magnetic configuration located beneath a multiarcade helmet streamer. We establish the sequence of activities appearance involved in casually linked chain of events on 2014 March 14: short-lived active region, surge eruption, EP BFR rising, EP BFR and MFR merging and interacting, EP common FR fast rise, flare, EP FR bifurcation, partial-halo CME with bi-component bright core, impulsive flare, post-flare loop arcade. A surge-like event in the northern EP footpoints is determined as the possible trigger of the bright FR appearance beneath the cool, massive FR. Plasma draining in this footpoints is identified as the precursor for the EP eruption. We find that the EP FRs merging at the fast-rise onset and their splitting in the phase of strong acceleration are the main triggers for the flaring activity. Studying the eruptions of EP hot and cool FRs with their associated CME, we find that they are co-spatial with the CME bright core, i.e. the hot and cool EP FRs produced bi-component CME bright core.

Key words: Sun; Solar Prominence Eruptions; Flares; Coronal Mass Ejections; Multi-wavelengt Observations

Introduction

The solar prominences (known as filaments, when they are observed on the disk) are dense and cool material suspended in the hot and thin solar corona along polarity inversion lines (PILs). They are found in magnetic dip regions located in two main magnetic configurations: a sheared arcade and a flux rope. In the sheared arcade configuration, the arcade connects the opposite polarities on either sides of a PIL, whereas in the case of the flux rope configuration the magnetic field has helical magnetic structure (Mackay et al., 2010). It is commonly accepted to divide filaments into three types according to their locations on the solar disk: active-region, intermediate, and quiescent filaments (e.g. Engvold, 1998; Mackay et al., 2010).

It is widely accepted that prominence/filament eruptions are often one aspect of a more general single eruption that can produce a solar flare and a coronal mass ejection (CME) (e.g., Hirayama, 1974; Shibata et al., 1995; Moore et al., 2001; Forbes, 2000; Priest & Forbes, 2002). These three eruptive phenomena are usually considered to be connected with each other, and they may be different manifestations of the same magnetic energy release process in the corona (e.g. Shibata et al., 1995; Forbes, 2000; Moore et al., 2001; Priest & Forbes, 2002; Sterling et al., 2012). Many studies of the relationship between eruptive prominences (EPs), solar flares and CMEs (e.g.,

Subramanian and Dere, 2001; Chandra et al., 2010) point out to strong relations between EPs and CMEs. Therefore, understanding the initiation and evolution of the EPs as one of the best proxies for CMEs provides a crucial physical understanding of the dynamical processes involved in CME initiation and evolution, with broader implications for space weather and geospace climate.

The formation, stability and eruption (or disappearance) of the filaments are nicely described in recent reviews (see, e.g. Schmieder et al., 2013; Parenti, 2014, Fan, 2014). Several basic mechanisms that can lead to the instability, trigger the energy release, and eruption of EPs have been proposed in many theoretical and numerical models, which can be divided in two groups. Two main mechanisms have been involved in the first group models: MHD ideal or non-ideal processes. The models of this group include kink (e.g. Hood & Priest, 1981; Fan and Gibson, 2004; Török and Kliem, 2005; Gibson and Fan, 2006a) and torus (e.g. Kliem & Török, 2006; Török and Kliem, 2007); Schrijver et al., 2008; Aulanier et al., 2010) instabilities of a twisted coronal flux rope structure. The second group models include resistive instabilities by flux cancellation and fast magnetic reconnections in current sheets: "breakout" reconnections (e.g. Antiochos et al., 1999; Sterling et a., 2001; Karpen et al., 2012), which require a multipolar magnetic flux system and "tether-cutting" reconnections (e.g. Moore and Roumeliotis, 1992; Moore et al., 2001), which can originate in a bipolar sheared system.

The occurrence of the two groups of instabilities may be caused by the evolution of the external magnetic field, such as magnetic cancellation (e.g. Chae et al., 2001; Sterling et al., 2007), magnetic emergence (e.g. Feynman & Martin, 1995), shearing motion (e.g. Aulanier et al., 2010) and the change of loops topology overlying the filament (e.g. Kong et al., 2013).

The interactions between two nearby filaments can cause their eruptions and can lead to a flare or CME (Jiang et al., 2014; Zhu et al., 2015; Yang et al., 2017 for reviews). Filaments interaction or merging via magnetic reconnection have been reported in some observational studies (e.g., Schmieder et al., 2004; Su et al., 2007; Kumar et al., 2010; Bi et al., 2012; Li & Ding, 2012; Liu et al., 2012; Kong et al., 2013) and modeled in numerical studies (e.g., Linton et al., 2001; DeVore et al., 2005; Aulanier et al., 2006; Török et al., 2007). Moreover, several recent observations showed that branches or threads of a filament can also interact and rapidly change the magnetic connectivity in the filament threads structure upon magnetic reconnection (Kim et al., 2001; Thompson, 2011; Bi et al., 2012; Liu et al., 2012).

In this paper we investigate the eruption of a solar prominence, using observations from Solar Dynamic Observatory (SDO) and Extreme Ultra-Violet Imager (EUVI) onboard the Solar Terrestrial Relations Observatory (STEREO) spacecraft. Thanks to the appropriate location of the two STEREO observatories at the time of observations (separation angle of 44 degrees between A and B) we have the opportunity to combine limb with on-disk observations. In Sect. 2 we describe the set of data used in this study. Sect. 3 presents the kinematics of the event as observed in the limb as prominence eruption and as filament on the disk. Particular attention is

paid to the accompanied flare activity, which is analyzed in Sect. 4. Sect. 5 describes the prominence eruption in relation to the associated CME. The main results from the present study are discussed in Sect. 6.

1 Observations and Data reduction

The EP on 2014 March 14 was observed above the eastern limb by SDO/AIA (Fig. 1) and above the western limb by STEREO A/EUVI. The event was observed in the STEREO B/EUVI FOV (Fig. 2) as a filament eruption near the western limb.

For the present study data from Atmospheric Imaging Assembly (AIA) on board the SDO were used. The AIA (Lemen et al., 2012) consists of seven Extreme Ultra-Violet (EUV) and three Ultra-Violet (UV) channels which provide an unprecedented view of the solar corona with an average cadence of ∼12 s. The AIA image field-of-view reaches 1.3 solar radii with a spatial resolution of ∼1.5″. For our analysis we used images taken with 12 s cadence in the 304 Å passband of AIA/SDO. To trace the EP evolution at different heights in the chromosphere and in the corona we used also images in 211 Å, 335 Å, 171 Å, 131 Å, 193 Å and 94 Å channels from AIA. We used level 1 reduced data, i.e. with the dark current removed and the flat-field correction applied.

We also analyzed observations from the EUVI onboard STEREO Behind (B) and Ahead (A) spacecraft (Howard et al., 2008). EUVI has a FOV of 1.7 $R\odot$ and observes in four spectral channels that cover the 0.1 to 20 MK temperature range (Kaiser et al., 2008). The EUVI detector has a pixel size of 1.6″. We used images in the He II 304 Å channel with an average cadence of 10 min from EUVI A, and in Fe XII/XXIV 195 Å channel with cadence of 10 min from EUVI B.

Images obtained by the Large Angle and Spectrometric Coronagraph (LASCO) C2 ($1.5-6R\odot$) and C3 ($3.7-30R\odot$) onboard SOHO (Brueckner et al., 1995) were also analyzed.

All the data were processed with the standard procedures, included in SolarSoftWare.

2 Prominence/filament eruption

2.1 Environment and pre-eruptive activities

The observations in all AIA/SDO channels show that the eruptive activity consisted of several eruptive events, which occurred on the eastern limb at average PA of 103°, e.g. at the site of EP between 04:30 UT and 21:30 UT.The prominence eruption started at 07:33 UT and lasted until 11:48 UT. In the EUVI B 195 Å channel the EP was observed as a filament eruption located along polarity inversion line in the young short-lived Active Region (AR) - SPoCa:SOL2014-03-14T04:08[1] still in its emergence phase.

[1] Identified by the Solar Object Locater (SOL) of the Heliophysics Events Knowledgebase (HEK; Martens et al, 2012)

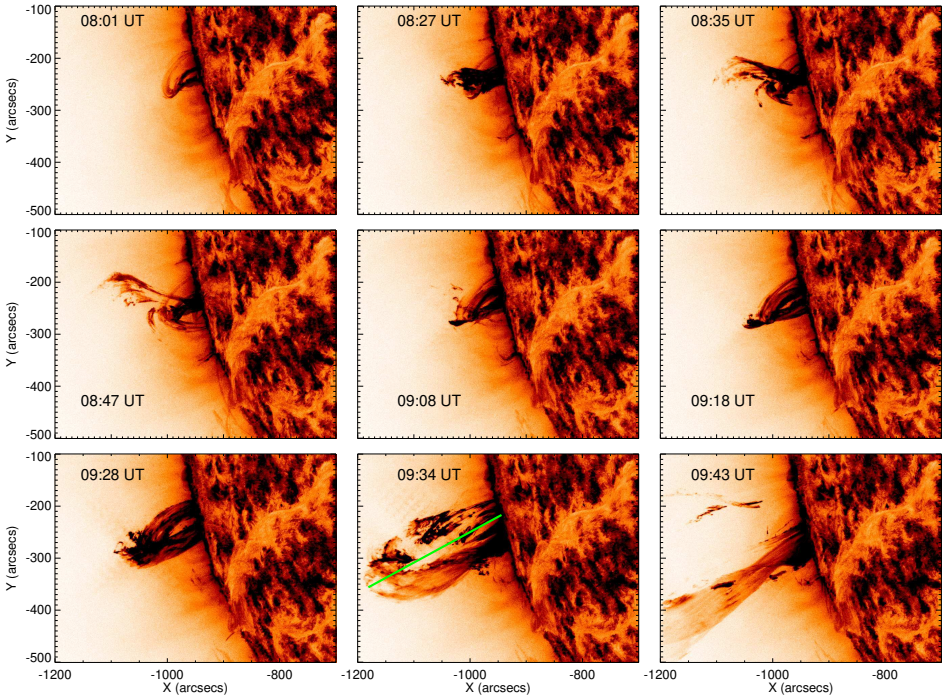

Fig. 1. The evolution of prominence eruption on 2014 March 14 in reversed color SDO/AIA 304 Å images. The green line marks the slice position used for height determination.

Moreover, the source filament region was situated at the bottom of a bipolar helmet streamer closely surrounded by two unipolar streamers that thus formed an unipolar-bipolar-unipolar ambient multiple-arcade helmet streamer (e.g. Yang et al. 2012). Six eruptions preceded or accompanied the filament eruption and the flare (see Table 1). These eruptions appeared ephemeral in AIA FOV but they played an important role in the pre-eruptive and eruptive filament activity and most probably they are sympathetically related both to each other and to the filament activation and eruption.

The EUVI B 195 Å images show that the slow rise of the filament (filament activation) started at 07:33 UT. The slow rising filament appeared on the limb as an EP in the AIA FOV at 08:01 UT (Fig. 1). A surge-like eruption (SLE) with 56-min duration started at 08:16 UT above the activity site (i.e., the EP site) in the AIA FOV. The SLE rose up along a trajectory that outlined overlying coronal loops (CLs). After the SLE onset (08:16 UT), because the EP and SLE were located at approximately the

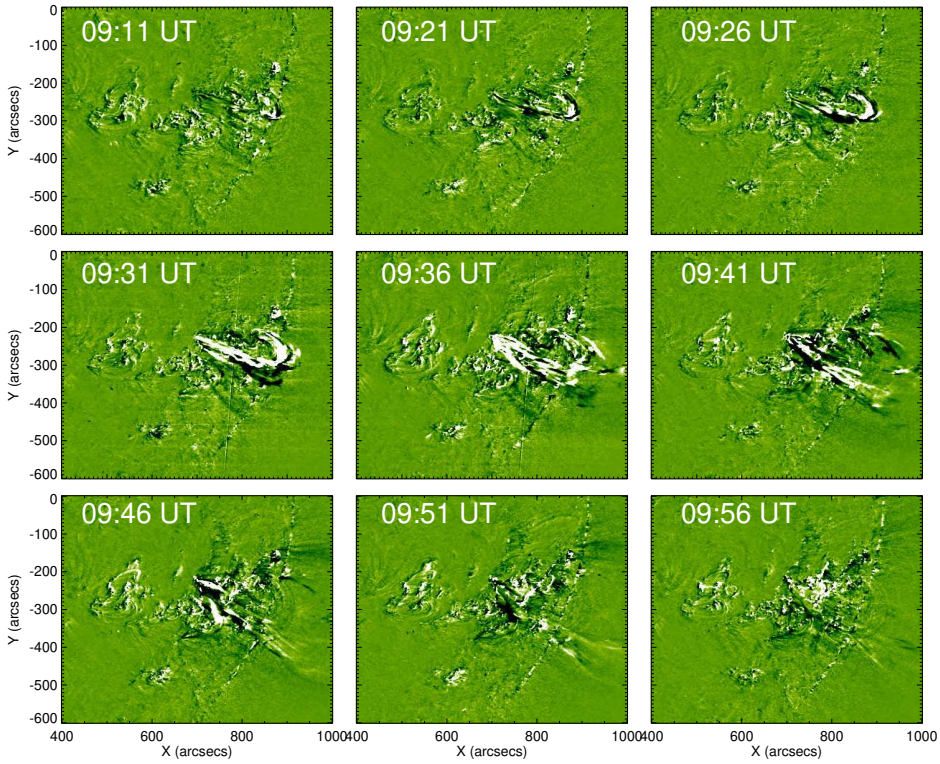

Fig. 2. The evolution of a filament on 2014 March 14 in STEREO B/EUVI 195 Å running difference images.

same PA, most of the EP slow rising above the limb was obscured by the bright SLE that was already in progress. At 08:52 UT the SLE reached a **maximum height** of 147 Mm (first low peak in Fig. 7) and then it started a down motion along the same trajectory, which was well expressed by its apparent plasma draining until 09:12 UT, when the surge-prominence completely disappeared. The filament slow rising continued until 09:16 UT and then it began to rise abruptly.

2.2 Prominence eruption

The EP remained complicated until 08:46 UT, when two magnetic flux ropes of the EP became recognizable (see Figs. 1 and 3). At 08:46 UT in AIA FOV one can clearly observe two FRs: one arch-like helically twisted massive FR (MFR) and another thin and bright one (BFR) that rose beneath the MFR (Fig. 3). At an earlier stage, at 08:40 UT, when the SLE

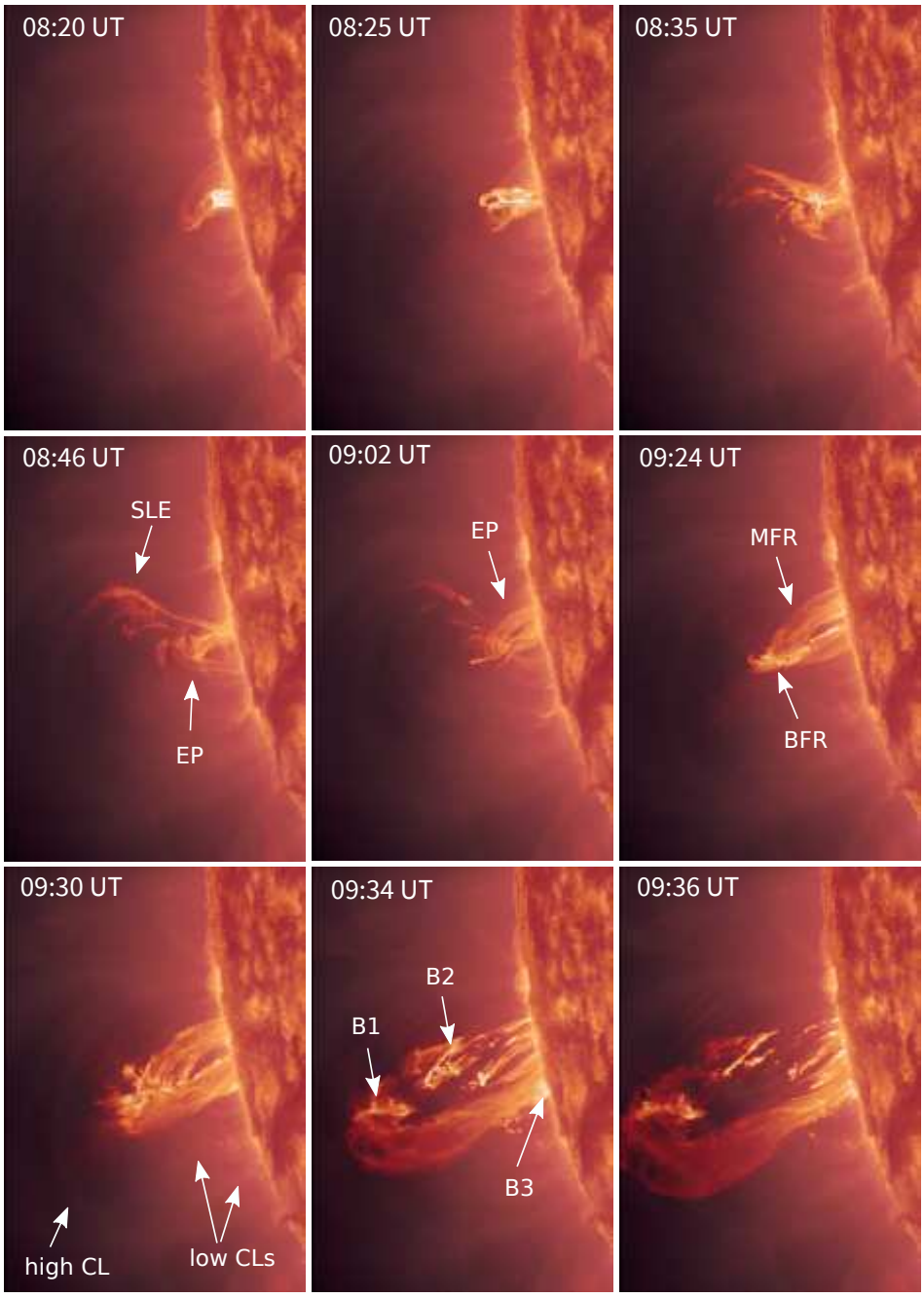

Fig. 3. SDO/AIA 304 Å and 211 Å combined images presenting basic stages in the evolution of the EP and its coronal environment.

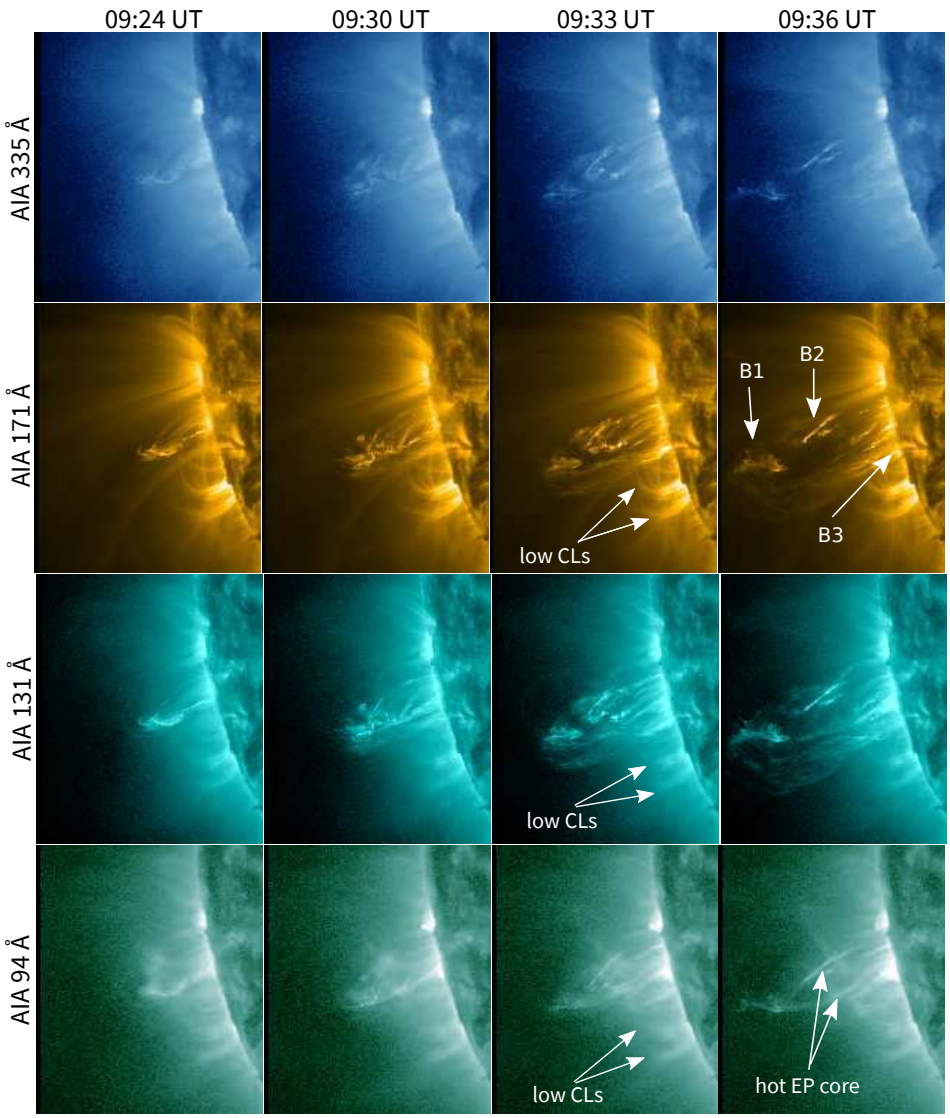

Fig. 4. Four stages in the evolution of the EP structure and brightening presented in the SDO/AIA 335 Å, 171 Å, 131 Å, and 94 Å high temperature channels.

plasma draining was already started, the BFR had a tightly twisted structure with a very bright footpoints, which were closely located to the northern feet of the MFR and the SLE feet, as well. After that time, the AIA images reveal that a brightening started at the BFR footpoints and continuously built up during the slow increase of the BFR height. The BFR underwent the changes in its shape between 08:40 UT and 09:18 UT. At

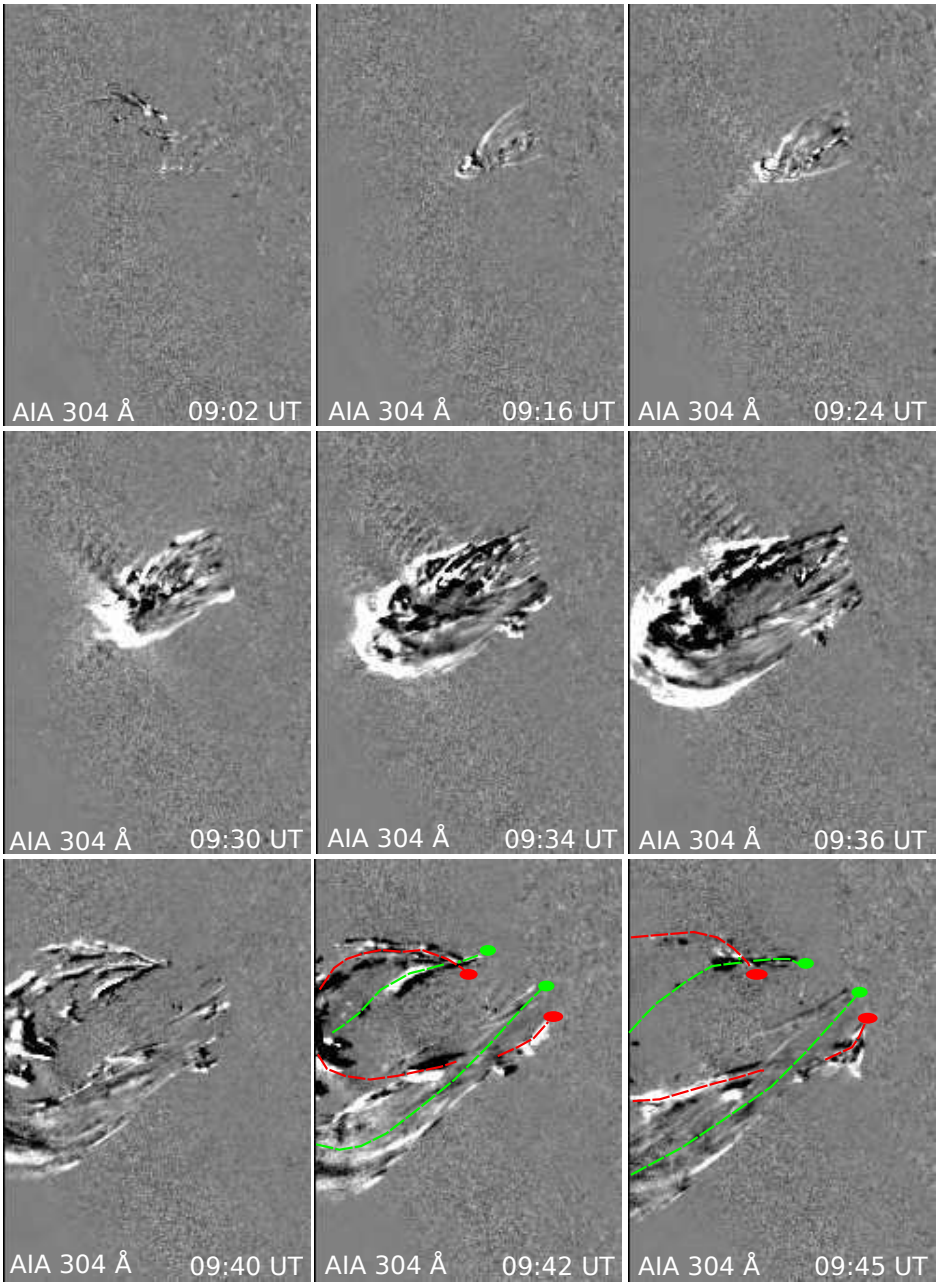

Fig. 5. SDO/AIA 304 Å running difference images presenting the main stages of the EP evolution. The dashed lines trace the loops of EP FRs: green - MFR and red - BFR. The green and red circles indicate the positions of the MFR and the BFR footpoints.

09:18 UT, just before the EP fast-rise phase, the BFR looked as a bright loop, which was tightly merged with the inner edge of arch-like MFR (see Fig. 1) that suggests a close interaction between the two FRs. Moreover, after 09:24 UT the two merged FRs rose coherently seeming as a single common FR (Fig. 3) that hereafter we will name EP.

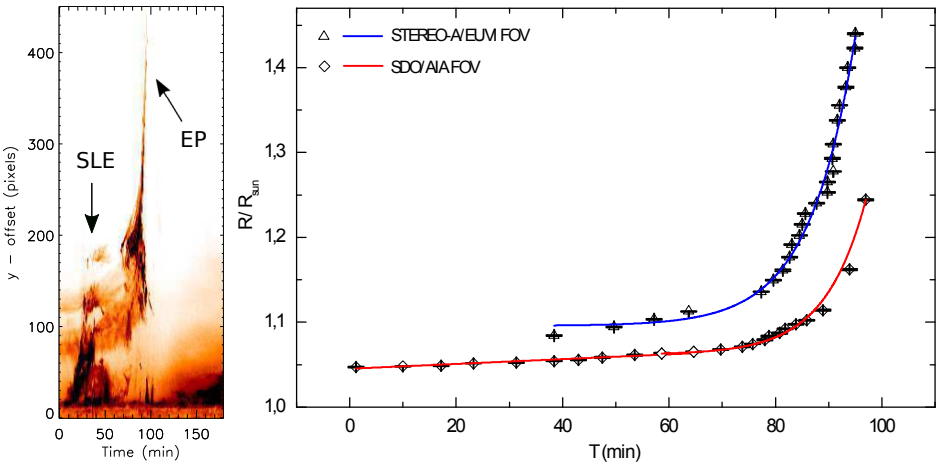

Fig. 6. left: Time-slice diagram used for height determination. **right**: Height-time diagram of prominence eruption as observed in AIA/SDO and STEREO A FOV.

After 09:16 UT the EP began rapidly to rise up and at 09:36 UT its summit escaped the AIA FOV, whereupon it was ejected high in the corona. After 09:36 UT, when the EP entered in a strong acceleration phase, the upper parts of MFR and BFR within the single FR began to split laterally. At 09:45 UT, when the EP summit escaped the AIA FOV, because of the structure simplification BFR exhibited at least two helically twisted thin threads (Fig. 1 and Fig. 5). At that time the upper parts of MFR and BFR became clearly recognizable because they sharply rose in different directions - MFR southeastwards and BFR northeastwards, respectively (Fig. 5). Afterwards, the angle between their propagation directions was at about 45°.

The evolution and coronal environment of the EP are given with more details in Fig. 3. Every panel in Fig. 3 combines two images with quite different temperatures: AIA 304 Å image (He II, ∼0.05 MK) that especially good highlights the location of cooler dense plasma (filaments or prominences) above the solar surface; AIA 211 Å (Fe XII, ∼1.25 MK) that highlights the corona and hot flare plasma. As one can see in Figs. 3 and 4, the EP rising took place beneath the coronal loops.

Figure 6, right panel, shows the time profiles of the EP height by limb observations of SDO/AIA 304 Å between 08:00 UT and 09:34 UT and STEREO-A/EUVI 304 Å between 08:38 UT and 09:35 UT. One can see in

the right panel of Fig. 6, that the EP clearly shows two distinctive phases: a slow rise phase and a fast acceleration phase. The slow rise phase lasted 62 minutes in the AIA FOV, between 08:00 UT and 09:02 UT. In the EUVI A FOV, only the end of EP slow raising was observed and it lasted 26 minutes (08:38 UT-09:04 UT) because the EP position was of $\sim 25^{\circ}$ behind the EUVI A western limb. In the AIA FOV the EP slowly rose with an average speed of $\sim$3 km s^{-1}. In the EUVI A FOV it rose with speeds from 2 km s^{-1} to 12 km s^{-1} at accelerations from 1 m s^{-2} to 11 m s^{-2}. During the fast phase as observed in the AIA FOV, the EP exponentially accelerated with speeds from $\sim$3.5 km s^{-1} to $\sim$280 km s^{-1}. In the EUVI FOV the eruptive phase was observed to bigger altitudes because of its bigger FOV (1.7 $R\odot$ vs 1.3 $R\odot$ of AIA FOV). The EP speeds increased from 12 km s^{-1} to 470 km s^{-1} at accelerations in the range 23-890 m s^{-2}.

Table 1. The activities involved in the event on 2014 March 14 (part of the events are detected by Solar Object Locater (SOL) of the Heliophysics Events Knowledgebase (HEK; Martens et al., 2012))

Events 2014-03-14 Activity	**Location about AIA disk center**	**Location Helio-coordinates**	**UT Start**	**UT End**
Active Region	-837.51; -356.47	L247C114	04:48:00	09:45:12
Filament Eruption	-1034; -304	L229C106	07:33:03	11:48:03
Eruption 1	-1030.8; -255.6	L229C103	08:09:52	08:49:52
Eruption 2	-1012.94; -252.28	L229C103	08:16:00	08:32:00
SLE	-1032.94; -244.68	L229C106	08:16:00	09:12:12
Eruption 3	-1026; -279.6	L229C105	08:54:40	09:34:40
Eruption 4	-1030.02; -282.97	L228C105	09:06:00	09:50:00
Eruption 5	-1136.4; -296.4	L228C104	09:16:00	09:56:00
Flare	-960; -268.8	L228C105	09:32:48	12:05:58
Eruption 6	-1122; -375.6	L229C108	09:35:12	10:15:12
CME		PA 85	10:00:05	16:30:06
Post-Flare Loops	-1032.2; -282.7	L229C108	10:49:43	20:38:43

3 EUV brightening of the EP and flare activity

For a detailed examination of the EP structure and brightening evolution combined AIA 304 Å and 211 Å images (Fig. 3) were used. The EP was also carefully examined in four high temperature AIA channels (Fig. 4): 335 Å (Fe XVI, $\sim$2.8 MK) that highlights active region and corona, 171 Å (Fe IX, $\sim$1 MK) that highlights coronal loops but also outlines the prominence magnetic tubes containing hot plasma, 131 Å (Fe VIII, Fe XXI; $\sim$10 MK, $\sim$18 MK) and 94 Å (Fe XVIII, $\sim$6 MK) that highlights solar flares.

The structure and brightening evolution of the EP was traced in Fig. 3, Fig. 4 and Fig. 6, which highlight mainly the temporal and spatial brightening dynamics that suggest an interaction between EP FRs and their heating (e.g. Joshi et al. 2016a) during early eruptive phase. At 09:10 UT

the narrow brightening in the top of EP began to enlarge and at 09:16 UT, just before the fast eruption it covered the whole FR top. The next eight minutes the top brightening and its morphology underwent changes. After 09:24 UT, probably due to reconnection heating, more and more threads revealed themselves from top to bottom and at 09:30 UT almost the whole EP was brightened (Fig. 3). After 09:30 UT, the EP underwent irregular spatial EUV dimming that affect mainly its northern leg, resulting in mix of dark and bright FR structures. It should be noted that the EP EUV dimming coincided with the flare onset (09:34 UT) (see Table 1). Subsequently, at 09:34 UT only two narrow regions of extreme brightening were observed at the EP top (B1) and in the middle part of the northern leg (B2), where a strong interaction between the EP FRs took place. The B1 and B2 brightening could be caused by the heating due to energy released from reconnection below the rising prominence (Su et al. 2015). An extreme EUV brightening was also observed at the footpoints of EP FRs (B3) (Fig. 3). The location of northern and southern footpoints near the outer boundary of the corresponding unipolar streamers suggests that their EUV brightening were observed as a signature of a current sheet formed at the leading edge of the EP, as distinct from the vertical current sheet beneath the EP, which is the source of post-flare arcade (Wang et al. 2009). This current sheet should be formed by reconnection occurring at the interface between the EP leading edge and the background corona, where strong currents are generated due to the compression and the rapid change in the direction of the field (e.g. Kliem et al. 2004). These extreme brightening features were well observed in the high temperature AIA channels, however, with some difference in magnitude (Fig. 4). Besides, only inner edge was visible in AIA 94 Å channel as an EP bright core.

The significant pre-eruption activities took place in the source region, such as evolution and activation of the short filament, and localized dynamic brightening from various locations close to the filament. In Fig. 7 we present the light curve of the EUVI B 195 Å integrated flux, that reveals two peaks. The first one is a low gradual peak with duration between 08:01 UT and 09:00 UT. It is most probably related to the interaction and brightening of several threads belonging to SLE, EP and low CLs because the peak maximum at 08:35 UT coincided with the time of strong EUV brightening of the interacting threads (see Fig. 3). The SLE, as a main event in this process, played crucial role, since just after 08:35 UT the EP BFR was activated. Later, the EUVI B 195 Å flux clearly indicates the onset of an impulsive flare emission at 09:52 UT, which almost coincided with the CME onset in the LASCO C2 FOV (10:00 UT) that is in conformity with the result of Zhang et al. (2001). Then, the emission sharply increased during the next 50 minutes and at 10:42 UT it reached a maximal value, just after the bifurcation of EP common FR. At that time, the MFR and BFR of EP were already visible as a spectacular, very bright CME core in the LASCO C2 FOV.

In contrast to the HEK registered flare that started at 09:32 UT and finished at 12:06 UT (Table 1), the impulsive flare took place close to the filament as observed in the EUVI B FOV. After its peak, at 10:50 UT the bright domed structure appeared on the limb in AIA FOV at the same

place where the EP appeared. Then, it began to rise up and at 14:15 UT it developed into post-flare loop arcade symmetrically extended along the filament (Fig. 8).

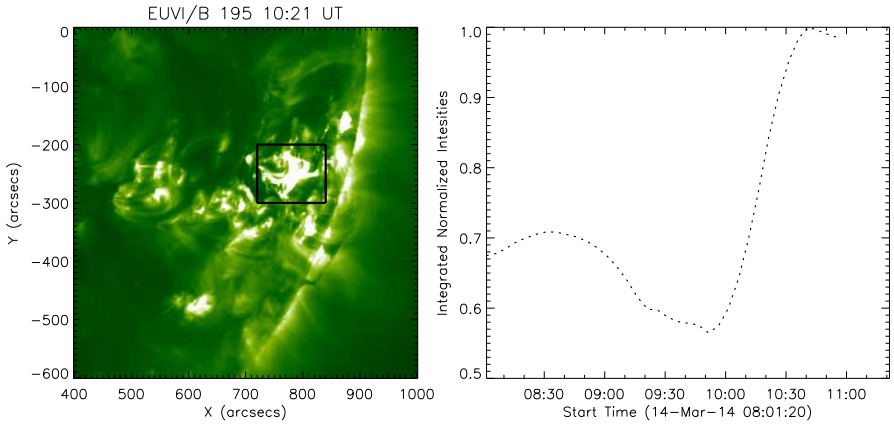

Fig. 7. left: EUVI B image in 195 Å channel; **right**: Integrated intensities in EUVI B 195 Å channel, obtained from the boxed region overplotted on the left panel.

4 Partial-halo CME

The partial-halo CME was observed by LASCO C2 and STEREO A/COR1 coronagrphs. A set of co-temporal AIA 304 Å and LASCO C2 images in Fig. 9 displays a few representative stages of the CME evolution. The CME was first seen on the eastern limb in LASCO C2 FOV at 10:00 UT appearing in the base of bipolar helmet streamer, at a PA of 85°. The EP upper part clearly appeared as CME bright core at 10:38 UT. The CME had a relatively faint leading front immediately followed by a bright loop. The bright core had two distinctive components: cool MFR and hot BFR. The first one, the upper part of MFR, was observed in the southern part of CME. The other one was very bright extensive region located in the northern CME part, whose centroid coincided with the EP BFR. Most probably, the high

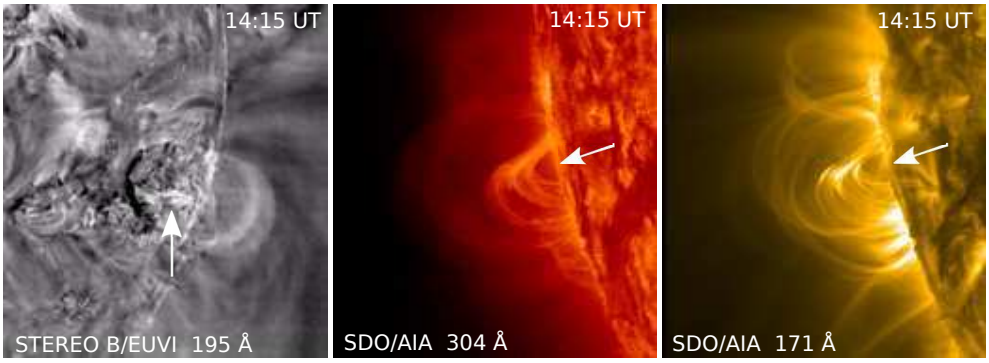

Fig. 8. A post-eruptive flare loops arcade on 2014 March 14 at 14:15 UT as observed in STEREO B/EUVI 195 Å running diference image and SDO/AIA 304 Å and 171 Å images. The white arrows point the EP limb position.

brightness was due to the interaction between the hot BFR and the ambient magnetic field (Su et al. 2015).

The southern core component (MFR) was bright until 11:02 UT when it reached a height of 3.5 $R\odot$. Afterwards, it began to gradually fade and remained distinguishable up to a height of $\sim$12 $R\odot$ in the LASCO C3 FOV at 16:00 UT. It has to be noted that a significant plasma downflow in the MFR southern leg was observed in the AIA FOV between 10:00 UT and 11:00 UT. Therefore, the plasma downflow could have a contribution to the fading of the CME cold component. At 11:35 UT the brightening evolution of CME loops finished and one can see that multiple arcade configuration was observed in the CME cavity. After that time, the bright region underwent gradual diminishing and between 12:35 UT and 13:35 UT the thin BFR was well observed and it can be traced up to a height of about 4.2 $R\odot$ (see Fig. 9). The two EP FRs were traced in the last four frames in Fig. 9, where the green line marks MFR and the red one denotes BFR.

The height-time profile of the partial-halo CME made by data of LASCO CME catalog is given in Fig. 10. The exact duration of all events that were involved in 2014 March 14 eruptive event are over-plotted in Fig. 10. The linear speed of CME propagation is about 469 km s^{-1}. A second-order fit to the height-time data indicates a velocity of 481 km s^{-1} and an acceleration of about 1 m s^{-2} in the propagation of CME. According to SOHO LASCO CME catalog, the CME reached a maximal width of 192° and a height of 19.2 $R\odot$.

5 Summary and Discussion

The sequence of eruptive activities involved in the 2014 March 14 event consisted of four chronological stages: (1) Pre-eruptive events that span the AR appearance and its early evolution, and the filament pre-eruptive changes; (2) An initial EP slow rise that span the surge eruption and the

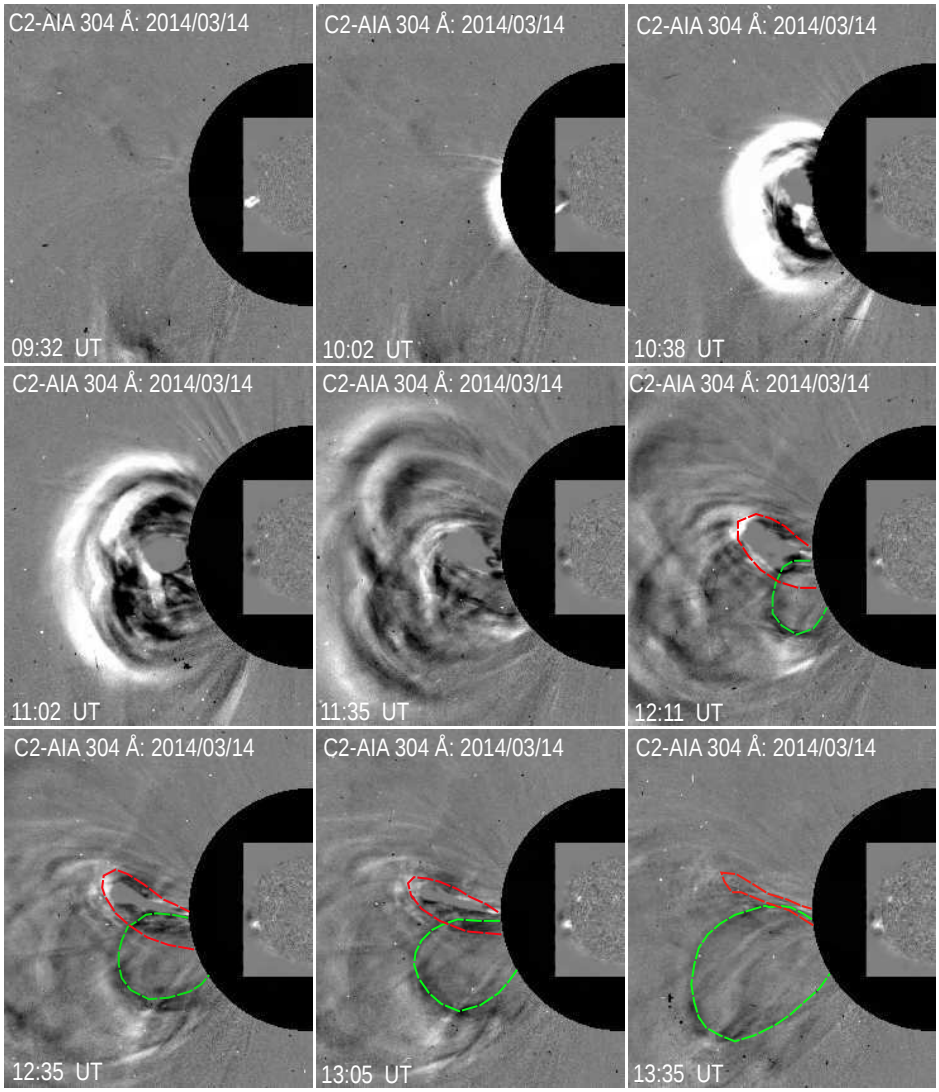

Fig. 9. A sequence of LASCO C2 and SDO/AIA 304 Å running difference images showing the progression of the 2014 March 14 prominence eruption as a bright core of partial-halo CME. The dashed lines in the last four frames trace the loops of EP FRs: green - MFR and red - BFR.

late slow rise phase of the filament observed as EP; (3) An EP fast-rise phase, when the EP massive and bright FRs sharply rose in the corona; (4) A CME evolution during which the impulsive flare occurs followed by a long-lasting post-eruptive arcade.

1. *Pre-eruptive events (04:30-08:00 UT).* The filament was located in-

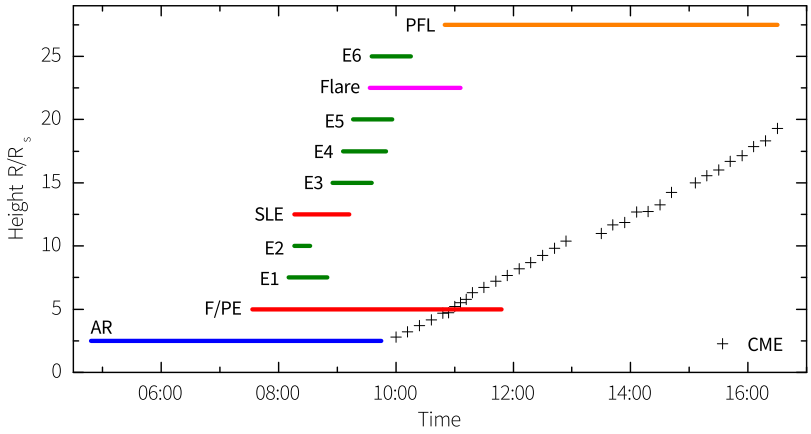

Fig. 10. Height-time diagram of the CME with the overplotted exact duration of all associated events.

side a confined arcade, wich was overlaid by a common arcade of the unipolar-bipolar-unipolar streamer belt. Therefore, our multiple-arcade streamer represents a favorable magnetic configuration for producing sympathetic events (Yang et al. 2012). The multipolar photospheric magnetic configuration around the filament, nearby young AR still in the emergence phase, and the gradual EUV emission under the slow rising filament as a precursor of slow magnetic reconnection (e.g. Moore et al. 2001; Joshi et al. 2016b) suggest a complex, multi-step process that produced a chain of a casually related surge, an EP, seven small eruptions, two flares, a partial-halo CME, and post-eruptive arcade.

2. *EP slow-rise (08:01-09:16 UT).* The continuous flux emergence in the young AR, as well as the associated flare suggest that the flux emergence could supply sufficient energy to trigger the SLE appearance at 08:16 UT (e.g., Shibata & Uchida 1986) by generation of low-altitude reconnection (Antiochos 1998; Pariat et al. 2010). Moreover, the surge could also generate an initially driven disturbances, which propagation continued after the surge's downflow onset (Zheng et al. 2012). In addition such disturbances could heat the plasma due to the kinetic energy of impacting surge material, or due to process of magnetic reconnection between the field carried by the impacting material and EP FRs. Such processes possibly acted in the magnetic field of low-lying loops close to the EP BFR, which is suggested by a strong brightening in EUVI B 195 Å light curve in Fig. 7 (see e.g. Gilbert et al. 2013). So that, the SLE is most reliable trigger of the EP BFR activation and its slow rising bellow the arch-like MFR. Moreover, the EUV brightening in all AIA channels responds at the same time and have similar decay times, which is an observational signature supporting the dominant role of the plasma compression over reconnection (Gilbert et al. 2013). During the surge plasma draining phase, except slow rising,

the BFR underwent slow rotation and brightening enhancement from the bottom upwards. Besides, the slow rise phase is characterized by an apparent plasma drainage that was observed in the threads of MFR and BFR. This stage finished just before the EP fast-rise onset, when the BFR was already visible as bright loop, which was merged with the MFR inner edge forming in this way a single common EP FR in the AIA FOV. There are two theoretically predicted mechanisms that could explain the merging of MFR and BFR. When the FRs are sufficiently close to each other, the force between them is comparable to or larger than the force of ambient field. Perturbations will then trigger a pinching of the X-type magnetic structure between the FRs. The subsequent reconnection at the formed current sheet will start redistributing the magnetic flux between the ropes and ambient field. This may cause the perturbation to grow and eventually to merge the FRs. This process depends on the properties of flux rope configuration and perturbation (Kliem et al. 2014). According to authors, this mechanism is reliable to merging if the lower FR show the stronger instability (as in our case). Another mechanism was predicted by simulations based on the Taylor relaxation model (Hussain et al. 2017), which can predict the energy release for FRs of different twist degrees, which relax individually or which merge through reconnection into a single FR. The authors found that the energy output of merging FRs dominated in the most strongly twisted rope. In addition, the very bright regions B1 and B2 that appeared during the next EP stage were composed of many tightly twisted threads with high degree of twisting, which suggests high energy release within them.

3. *EP fast-rise (09:16-10:00 UT).* This stage contained two specific sub-stages: first one of coherent, rapid rising of a single EP FR between 09:16 UT and 09:32 UT, and second one of sharp EP rising and bifurcation of the single FR between 09:32 UT and 09:41 UT. An essential feature of the first sub-stage was the dynamic EP EUV brightening, suggesting an interaction between merged FRs within the common FR. The initial EP top brightening began to spread down probably due to reconnection heating (e.g. Joshi et al. 2016a) and at 09:30 UT almost the whole EP was brightened. The second sub-stage started with fragmentation of the EP brightening due to EUV dimming in different part of EP FR and at 09:34 UT only three regions of strong EUV emission remained in the EP: at the top (B1), in the middle part of northern leg (B2), and at FR footpoints (B3). These regions contained strongly heated plasma because they were well visible in all AIA channels, especially in the high temperature. The extreme EUV footpoint brightening could be interpreted as an evidence for magnetic reconnection between the rapidly ascending EP and the overlying coronal arcade (e.g. Kliem et al. 2004). Such leading-edge reconnection involves the EP itself and is driven by its eruption. Note, that this process is distinct from the reconnection that occurs beneath the EP, which produces the post-flare arcade (Wang et al. 2009). In addition, during the EUV dimming process a flare started at 09:32 UT in the EP vicinity that suggests a sympathetic casual relation between the EP and the flare. The second sub-stage started with EP FR bifurcation and at 09:41 UT the massive and bright FRs were again visible, but well separated, with propagations in quite different directions. It started just after the strong acceleration onset of EP, when the upper part of its single FR began to split laterally, which is like the cases

of partial eruptions (e.g. Gibson & Fan 2006b; Gilbert et al. 2001, 2007; Liu et al. 2007). The splitting of MFR and BFR within the single FR could be explained by the transfer of magnetic flux from the lower to the upper rope (Kliem et al. 2014). Moreover, in some extent our case is in conformity with the scenarios of Kliem et al. (2014) for full eruption of the double-FR, in which the dominant instability of lower FR revealing as upward perturbation is applied to upper FR. According to Kliem et al. (2014) such full eruption is clearly driven by the stronger torus instability of the lower flux rope and is very similar to the eruption of a single torus-unstable flux rope.

4. *A CME evolution (10:00 UT - 20:49 UT).* The basic eruptive events that appeared in this stage were a partial-halo CME, an impulsive flare, and a post-eruptive arcade. The CME surrounded multiarcade helmet streamer and by this reason it had some specific features with respect to the classical CME three-parts structure. The CME leading front loop was relatively faint followed by the secondary apparent bright loop, and cavity bellow them, which was insufficiently revealed because of its multiarcade system. The CME bright core presented a bi-component structure produced by the upper parts of cool MFR and hot BFR, which had quite different asymmetrical positions in the cavity. Such bright core with hot and cool components was reported for the first time by Li and Zhang (2013) from on-disk observations of a filament eruption. After the bifurcation of EP common FR, the MFR began to propagate in direction close to those of the southern unipolar streamer, while the thin BFR propagated bellow the bipolar streamer. The MFR upper part gradually faded with its growth, while the BFR underwent strong brightening. Three possible types of interactions could be responsible for such brightening: (1) between BFR and the ambient field of bipolar streamer (Cohen et al. (2010)), (2) between closed magnetic fields of bipolar streamer and overlying CME bright loop that could change the connectivity in overlying arcade (Cohen et al. (2010)), (3) between the bipolar streamer and the open field of northern unipolar streamer (Zhu et al. (2014); Yang et al. (2015)). The impulsive flare started at 09:52 UT, just after the EP bifurcation and almost simultaneously with the CME appearance (10:02 UT) in the LASCO C2 FOV. It reached maximum at the time when extensive strong brightening in the bipolar region containing BFR was observed. Moreover, the flare maximum almost coincided with the post-flare loops appearance on the limb in AIA FOV. The post-flare loops reached maximal height at 16:00 UT and its evolution lasted until 20:49 UT.

In conclusion, we reported the evolution of an EP on 2014 March 14 composed by both hot BFR and cool MFR, which involved a rare feature of interaction between the BFR and MFR that subsequently appeared as bi-component bright core in the associated partial-halo CME. Moreover, we emphasize that the EP was part of a chain of physically linked sympathetic events appearing in a single region below the multiarcade helmet streamer between 04:30 UT and 21:00 UT. The chronological sequence of the successive destabilizations taking place in the region is: AR appearance - surge eruption - EP BFR appearing and rising - EP BFR and MFR merging - EP common FR fast rise - flare - EP FR bifurcation - partial-halo CME - impulsive flare - post-flare loop arcade. Since the various types of eruptive activity were involved in this chain, we here focused mainly on the EP evo-

lution. The detail CME evolution, impulsive flare and post-flare loops will be subjects of a further investigation.

Acknowledgments

This research was partially supported by the Bulgarian National Science Fund of the Ministry of Education and Science under grant DN 08-1/2016.

References

Antiochos, S. K., 1998, *ApJ* **502**, L181
Antiochos, S. K.; DeVore, C. R.; Klimchuk, J. A., 1999, *ApJ* **510**, 48
Aulanier G., Török, T., Dèmoulin P., DeLuca E. E., 2010, *ApJ* **708**, 314
Aulanier, G.; DeVore, C. R.; Antiochos, S. K., 2006, *ApJ* **646**, 1349
Bi, Y.; Jiang, Y.; Li, H.; Hong, J.; Zheng, R., 2012, *ApJ* **758**, 42
Brueckner, G. E.; Howard, R. A.; Koomen, M. J.; Korendyke, C. M, et al., 1995, *Sol. Phys.*, **162**, 357
Chae J.; Wang H.; Qiu J.; Goode P. R.; Strous L.; Yun H. S., 2001, *ApJ* **560**, 476
Chandra, R.; Pariat, E.; Schmieder, B.; Mandrini, C. H.; Uddin, W., 2010, *Sol. Phys.* **261**, 127
Cohen, O., Attrill, G. D. R., Schwadron, N. A., Crooker, N. U., Owens, M. J., Downs, C., Gombosi, T. I., 2010, *JGR* **115**, A10104
DeVore, C. R.; Antiochos, S. K.; Aulanier, G., 2005, *ApJ* **629**, 1122
Engvold, O., 1998, in IAU Colloq. 167, *New Perspectives on Solar Prominences*, ed. D. F. Webb, B. Schmieder & D. M. Rust, ASP CS, Vol. 150, 23
Fan, Y. & Gibson, S. E., 2004, *ApJ* **609**, 1123
Fan, Y., Chapter 12 *MHD Equilibria and Triggers for Prominence Eruption.* In J.C. Vial, O. Engvold (eds.) *Solar Prominences*, Springer (2014)
Feynman, J. & Martin, S. F., 1995, *J. Geophys. Res.* **100**, 3355
Forbes T. G., 2000, *J. Geophys. Res.* **105**, 23153
Gibson, S. E. & Fan, Y., 2006a, *J. Geophys. Res.* **111**, A12103
Gibson, S. E., & Fan, Y., 2006b, *ApJ* **637**, L65
Gilbert, H. R., Holzer, T. E., Burkepile, J. T., 2001, *ApJ* **549**, 1221
Gilbert, H. R., Alexander, D., Liu, R., 2007, *Sol. Phys.* **245**, 287
Gilbert, H. R., Inglis, A. R., Mays, M. L., Ofman, L., Thompson, B. J., and Young, C. A., 2013, *ApJ* **776**, L12
Hirayama, T., 1974, *Sol. Phys.* **34**, 323
Hood, A. W. & Priest, E. R., 1981, *Geophysical and Astrophysical Fluid Dynamics* **17**, 297
Howard, R. A.; Moses, J. D.; Vourlidas, A., et al., 2008, *SSRv*, **136**, 67
Hussain, A. S.; Browning, P. K.; Hood, A. W., 2017, *A&A* **600**, 11
Jiang, Y.; Yang, J.; Wang, H.; et al., 2014, *ApJ* **793**, 14
Joshi, Navin Chandra; Schmieder, Brigitte; Magara, Tetsuya; Guo, Yang; Aulanier, Guillaum, 2016a, *ApJ* **820**, 126
Joshi, Bhuwan; Kushwaha, Upendra; Veronig, Astrid M.; Cho, K.-S., 2016b, *ApJ* **832**, 130
Kaiser, M. L.; Kucera, T. A.; Davila, J. M.; St. Cyr, O. C.; Guhathakurta, M.; Christian, E., 2008, *SSRv*, **136**, 5
Karpen, J. T.; Antiochos, S. K.; DeVore, C. R., 2012, *ApJ* **760**, 81
Kim J.-H.; Yun H. S.; Lee S.; Chae J.; Goode P. R.; Wang H., 2001, *ApJ* **547**, 85
Kliem, B. & Török, T., 2006, *Phys. Rev. Lett.* **96**, 255002
Kliem, B., Titov, V. S., & Török, T., 2004,*A&A* **413**, L23
Kliem, B., Török, T., Titov, V. S., Lionello, R., Linker, J. A., Liu, R., Liu, C., Wang, H., 2014, *ApJ* **792**, 107
Kong, D. F.; Yan, X. L.; Xue, Z. K., 2013, *Ap&SS* **348**, 303
Kumar, P.; Manoharan, P. K.; Uddin, W., 2010, *ApJ* **710**, 1195
Lemen, J. R., Title, A. M., Akin, D. J., et al., 2012, *Sol. Phys.*, **275**, 17
Li, Y. & Ding, M.-D. 2012, *RAA* **12**, 287
Li, L. P. & Zhang, J., 2013 *A&A* **552**, L11

Linton, M. G.; Dahlburg, R. B.; Antiochos, S. K., 2001, *ApJ* **553**, 905
Liu, R., Alexander, D., Gilbert, H. R., 2007, *ApJ* **661**, 1260
Liu, R.; Kliem, B.; Török, T.; et al., 2012, *ApJ* **756**, 59
Mackay, D. H.;, Karpen, J. T.; Ballester, J. L.; Schmieder, B.; Aulanier, G., 2010, *SSRv* **151**, 333
Martens, P.C.H., Attrill, G.D.R., Davey, A.R., Engell, A., et al., 2012, *Sol. Phys.*, **275**, 79
Moore, R.L. & Roumeliotis, G., 1992, in IAU Colloq. 133, *Eruptive Solar Flares*, (Eds.) Svestka, Z., Jackson, B.V., Machado, M.E., LNP Vol. 399, pp. 69–78, Springer
Moore, R. L.; Sterling, A. C.; Hudson, H. S.; Lemen, J. R., 2001, *ApJ* **552**, 833
Parenti, S., 2014, *Living Reviews in Solar Physics* **11**, 1
Pariat, E., Antiochos, S. K., DeVore, C. R., 2010, *ApJ* **714**, 1762
Priest E. R. & Forbes T. G., 2002, *A&AR* **10**, 313
Schmieder, B.; Dèmoulin, P.; Aulanier, G., 2013, *Advances in Space Research* **51**, 1967
Schmieder, B.; Mein, N.; Deng, Y.; et al., 2004, *Sol. Phys.* **223**, 119
Shibata, K.; Masuda, K.; Shimojo, M.; et al., 1995, *ApJ* **451**, L83
Shibata, K. & Uchida, Y., 1986, *Sol. Phys.* **103**, 299
Schrijver, C. J.; Elmore, C.; Kliem, B., Török, T.; Title, M., 2008, *ApJ* **674**, 586
Sterling, A. C.; Moore, R. L.; Berger, T. E.; Bobra, M.; et al., 2007, *PASJ* **59**, 823
Sterling, A. C.; Moore, R. L.; Hara, H., 2012, *ApJ* **761**, 69
Sterling, A. C.; Moore, R. L.; Qiu, J.; Wang, H., 2001, *ApJ* **561**, 1116
Su, J.; Liu, Y.; Kurokawa, H.; et al., 2007, *Sol. Phys.* **242**, 53
Su, Yingna; van Ballegooijen, Adriaan; McCauley, Patrick; Ji, Haisheng; Reeves, Katharine K.; DeLuca, Edward E., 2015, *ApJ* **807**, 144
Subramanian, P. & Dere, K. P., 2001. *ApJ* **561**, 372
Thompson, W. T., 2011, *JASTP* **73**, 1138
Török, T. & Kliem, B., 2005, *ApJ* **630**, L97
Török, T. & Kliem, B., 2007, *Astron. Nachr.* **328**, 743
Wang, Y.-M., Muglach, K., & Kliem, B. 2009, *ApJ* **699**, 133
Yang, Liheng; Yan, Xiaoli; Li, Ting; Xue, Zhike; Xiang, Yongyuan, 2017, *ApJ* **838**, 131
Yang, J., Jiang, Y., Zheng, R., et al. 2012, *ApJ* **745**, 9
Yang, J., Jiang, Y., Xu, Z., Bi, Y., Hong, J., 2015, *ApJ* **803**, 68
Zhang, J., Dere, K. P., Howard, R. A., Kundu, M. R., White, S. M., 2001, *ApJ* **559**, 452
Zheng, R., Jiang, Y., Yang, J., et al., 2012, *ApJ* **747**, 67
Zhu, C., Alexander, D., Sun, X., Daou, A., 2014, *Sol. Phys.* **289**, 4533
Zhu, C.; Liu, R.; Alexander, D.; Sun, X.; McAteer, R. T. J., 2015, *ApJ* **813**, 60